

THREE-DIMENSIONAL COMPUTATIONAL FLUID DYNAMICS ANALYSIS OF BUOYANCY-DRIVEN NATURAL VENTILATION AND ENTROPY GENERATION IN A PRISMATIC GREENHOUSE

by

**Walid AICH^{a,b}, Lioua KOLSI^{a,b}, Mohamed N. BORJINI^b,
Abdullah A. A. AL-RASHED^c, Habib Ben AISSIA^b,
Hakan F. OZTOP^{d,e,*}, and Nidal ABU-HAMDEH^e**

^a College of Engineering, Hail University, Hail City, Saudi Arabia

^b Research Unit for Metrology and Energy Systems, National Engineering Scholl of Monastire,
University of Monastir, Monastir, Tunisia

^c Department of Automotive and Marine Engineering Technology, College of Technological Studies,
the Public Authority for Applied Education and Training, Adailiyah, Kuwait

^d Department of Mechanical Engineering, Technology Faculty, Firat University, Elazig, Turkey

^e Department of Mechanical Engineering, King Abdulaziz University, Jeddah, Saudi Arabia

Original scientific paper

<https://doi.org/10.2298/TSCI151015052A>

A computational analysis of the natural ventilation process and entropy generation in 3-D prismatic greenhouse was performed using CFD. The aim of the study is to investigate how buoyancy forces influence air-flow and temperature patterns inside the greenhouse having lower level opening in its right heated façade and also upper level opening near the roof top in the opposite cooled façade. The bottom and all other walls are assumed to be perfect thermal insulators. Rayleigh number is the main parameter which changes from 10^3 to 10^6 and Prandtl number is fixed at $Pr = 0.71$. Results are reported in terms of particles trajectories, iso-surfaces of temperature, mean Nusselt number, and entropy generation. It has been found that the flow structure is sensitive to the value of Rayleigh number and that heat transfer increases with increasing this parameter. Also, it have been noticed that, using asymmetric opening positions improve the natural ventilation and facilitate the occurrence of buoyancy induced upward cross air-flow (low-level supply and upper-level extraction) inside the greenhouse.

Key words: 3-D CFD, natural ventilation, prismatic greenhouse, heat transfer, entropy generation

Introduction

Ventilation is essential for a good climate in a greenhouse and great effort has been made for the determination of ventilation quality as a function of relevant parameters. The most unfavorable situation for greenhouse cooling occurs when the wind speed is low, and natural ventilation is predominantly driven by buoyancy forces. Several studies on natural ventilation have been performed in the past. However, a detailed review of the literature indicates that the majority of these studies focused on 2-D models, thus ignoring the 3-D characteristics of flow and temperature distribution in the greenhouse. Also, there is a lack of re-

* Corresponding author, e-mail: hfoztop1@gmail.com

search that analyzes the impact of asymmetric opening positions and roof inclination on natural ventilation potential. Since the pioneer CFD works of Okushima *et al.* [1], most studies [2-12] concerning the distributed climate inside greenhouses have adopted a 2-D representation. Kacira *et al.* [13] observed that the utilization of side vents combined with roof vents minimized the temperature difference between the greenhouse air temperature and the outside temperature (compared with greenhouses with roof vents alone), and provided more uniform climate distribution inside the greenhouse. Kacira *et al.* [14] conducted 2-D simulations on two- and four-span sawtooth greenhouses. For two-span greenhouses with windward side openings and leeward roof vents, they reported that for wind velocities in the range of 1-2 m/s, outside air enters the greenhouse through the windward side opening and primarily crosses the greenhouse from one side to another. When there is no side opening, fresh air mainly enters through the roof vent located upstream but exits through both roof openings. The authors concluded that the ventilation is maximal when a windward side opening is combined with leeward roof vents. Lo and Novoselac [15] pointed out that the position of the outlet opening at the leeward façade only has a small impact on the volume flow rate, however, they analyzed a position of the outlet opening that is at the same level as the inlet opening, which is not the case in the current study. Aich *et al.* [16] carried out a 2-D numerical study of natural convection flows in a prismatic cavity. It has been found that a considerable proportion of the heat transfer across the inclined walls of the enclosure takes place near the intersection of the adiabatic vertical walls and cold inclined walls. Also, it has been noticed that, in a cavity still receiving a uniform heat flux, the bottom is not isothermal and the flow structure is sensitive to the cavity's shape. Many re-circulation zones can occur in the core of the cavity and the heat transfer is dependent on the flow structure. Oztop *et al.* [17] conducted on 3-D buoyancy and thermocapillary convection in an enclosure. They found that Marangoni number becomes more effective parameter on total entropy generation for lower values of Rayleigh numbers. Kolsi *et al.* [18] performed 3-D numerical analyses of laminar mixed convection and entropy generation in a cubic lid-driven cavity. It was found that direction of lid is an effective parameter on both entropy generation and heat- and fluid-flow for low values of Richardson number but it becomes insignificant at high Richardson number. This review of the literature shows that CFD has developed into a powerful tool for studies in urban physics and building aerodynamics, including natural ventilation in buildings, as demonstrated by review papers [19, 20].

The paramount aim of this work is to investigate the buoyancy-driven natural ventilation and entropy generation inside prismatic greenhouse, equipped with lower level opening in its right heated façade and upper level opening near the roof top in the opposite cooled façade, using 3-D CFD.

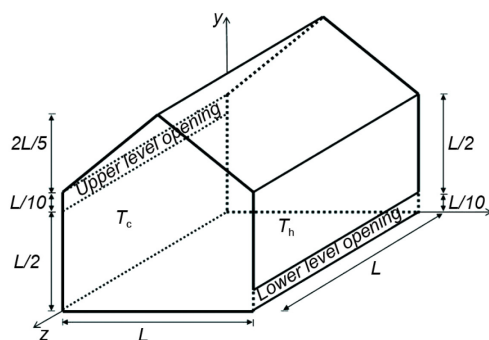


Figure 1. Schematic of an air-filled prismatic greenhouse

Mathematical formulation

Physical model

Physical model is presented in fig. 1 with co-ordinates. The considered problem is 3-D buoyancy-driven natural ventilation and entropy generation inside prismatic greenhouse having lower level opening in its

right heated facade at constant temperature T_h and also upper level opening near the roof top in the opposite cooled façade at constant temperature T_c . The bottom and all other walls are insulated.

Governing equations and numerical solution

Formalism $(\vec{\psi} - \vec{\omega})$ which are, respectively, defined by the two following relations, is used:

$$\vec{\omega}' = \vec{\nabla} \times \vec{V}' \quad \text{and} \quad \vec{V}' = \vec{\nabla} \times \vec{\psi}' \quad (1)$$

The setting in equation is described with more detail in [21]. After adimensionalization the system of equations controlling the phenomenon becomes:

$$-\vec{\omega} = \nabla^2 \vec{\psi} \quad (2)$$

$$\frac{\partial \vec{\omega}}{\partial t} + (\vec{V} \nabla) \vec{\omega} - (\vec{\omega} \nabla) \vec{V} = \Delta \vec{\omega} + \text{Ra Pr} \left[\frac{\partial T}{\partial z}, \quad 0, \quad -\frac{\partial T}{\partial x} \right] \quad (3)$$

$$\frac{\partial T}{\partial t} + \vec{V} \nabla T = \Delta T \quad (4)$$

with $\text{Pr} = \nu/\alpha$ and $\text{Ra} = (g\beta\Delta TL^3)/\nu\alpha$.

Boundary conditions for considered model are given:

Temperature

$$T = 1 \text{ at } x = 1 \text{ and } T = 0 \text{ at } x = 0$$

$$\frac{\partial T}{\partial n} = 0 \text{ on all other walls (adiabatic)}$$

$$T_{\text{in}} = T_c \quad \text{if} \quad \vec{n} \cdot \vec{V} < 0$$

$$\left. \frac{\partial T}{\partial n} \right|_{\text{out}} = 0 \quad \text{if} \quad \vec{n} \cdot \vec{V} \geq 0$$

Velocity

$$V_x = V_y = V_z = 0 \text{ on all walls}$$

$$\frac{\partial V_x}{\partial x} = \frac{\partial V_y}{\partial x} = \frac{\partial V_z}{\partial x} = 0 \text{ at open boundary}$$

Vorticity

$$\omega_x = 0, \quad \omega_y = -\frac{\partial V_z}{\partial x}, \quad \omega_z = \frac{\partial V_y}{\partial x} \quad \text{at } x = 0 \text{ and } 1$$

$$\omega_x = \frac{\partial V_z}{\partial y}, \quad \omega_y = 0, \quad \omega_z = -\frac{\partial V_x}{\partial y} \quad \text{at } y = 0 \text{ and } 1$$

$$\omega_x = -\frac{\partial V_y}{\partial z}, \quad \omega_y = \frac{\partial V_x}{\partial z}, \quad \omega_z = 0 \quad \text{at } z = 0 \text{ and } 1$$

Vector potential

$$\frac{\partial \psi_x}{\partial x} = \psi_y = \psi_z = 0 \quad \text{at } x = 0 \text{ and } 1$$

$$\psi_x = \frac{\partial \psi_y}{\partial y} = \psi_z = 0 \quad \text{at } y = 0 \text{ and } 1$$

$$\psi_x = \psi_y = \frac{\partial \psi_z}{\partial z} = 0 \quad \text{at } z = 0 \text{ and } 1$$

The generated entropy is written in the following form:

$$S'_{\text{gen}} = -\frac{1}{T'^2} \bar{q} \bar{\nabla} T' + \frac{\mu}{T'} \phi'$$

The first term represents the generated entropy due to temperature gradient and the second that due to the friction effects:

$$\bar{q} = -k \cdot \text{grad} T$$

The dissipation function is written in incompressible flow as

$$\begin{aligned} \phi' = 2 & \left[\left(\frac{\partial V'_x}{\partial x'} \right)^2 + \left(\frac{\partial V'_y}{\partial y'} \right)^2 + \left(\frac{\partial V'_z}{\partial z'} \right)^2 \right] + \\ & + \left(\frac{\partial V'_y}{\partial x'} + \frac{\partial V'_x}{\partial y'} \right)^2 + \left(\frac{\partial V'_z}{\partial y'} + \frac{\partial V'_y}{\partial z'} \right)^2 + \left(\frac{\partial V'_x}{\partial z'} + \frac{\partial V'_z}{\partial x'} \right)^2 \end{aligned} \quad (5)$$

from where the generated entropy is written:

$$\begin{aligned} S'_{\text{gen}} = \frac{k}{T_0'^2} & \left[\left(\frac{\partial T'}{\partial x'} \right)^2 + \left(\frac{\partial T'}{\partial y'} \right)^2 + \left(\frac{\partial T'}{\partial z'} \right)^2 \right] + 2 \frac{\mu}{T_0'} \\ & \left\{ \left(\frac{\partial V'_x}{\partial x'} \right)^2 + \left(\frac{\partial V'_y}{\partial y'} \right)^2 + \left(\frac{\partial V'_z}{\partial z'} \right)^2 + \left(\frac{\partial V'_y}{\partial x'} + \frac{\partial V'_x}{\partial y'} \right)^2 + \left(\frac{\partial V'_z}{\partial y'} + \frac{\partial V'_y}{\partial z'} \right)^2 + \left(\frac{\partial V'_x}{\partial z'} + \frac{\partial V'_z}{\partial x'} \right)^2 \right\} \end{aligned} \quad (6)$$

After adimensionalisation one obtains generated entropy number (dimensionless local entropy generated) which is written in the following way:

$$N_s = S'_{\text{gen}} \frac{1}{k} \left(\frac{L T_0}{\Delta T} \right)^2 \quad (7)$$

from where:

$$N_s = \left[\left(\frac{\partial T}{\partial x} \right)^2 + \left(\frac{\partial T}{\partial y} \right)^2 + \left(\frac{\partial T}{\partial z} \right)^2 \right] +$$

$$+ \varphi \left\{ 2 \left[\left(\frac{\partial V_x}{\partial x} \right)^2 + \left(\frac{\partial V_y}{\partial y} \right)^2 + \left(\frac{\partial V_z}{\partial z} \right)^2 \right] + \left(\frac{\partial V_y}{\partial x} + \frac{\partial V_x}{\partial y} \right)^2 + \left(\frac{\partial V_z}{\partial y} + \frac{\partial V_y}{\partial z} \right)^2 + \left(\frac{\partial V_x}{\partial z} + \frac{\partial V_z}{\partial x} \right)^2 \right\} \quad (8)$$

with $\varphi = (\mu\alpha^2 T_m)/(l^2 k \Delta T^2)$ is the irreversibility coefficient.

The first term of N_s represents the local irreversibility due to the temperatures gradients, it is noted N_{s-th} . The second term represents the contribution of the viscous effects in the irreversibility it is noted N_{s-fr} . The N_s gives a good idea on the profile and the distribution of the generated local dimensionless entropy. The total dimensionless generated entropy is:

$$S_{tot} = \int_v N_s dv = \int_v (N_{s-th} + N_{s-fr}) dv = S_{th} + S_{fr} \quad (9)$$

The local and average Nusselt numbers at the cold wall are given by:

$$Nu = \frac{\partial T}{\partial x} \Big|_{x=1} \quad \text{and} \quad Nu_m = \int_0^{L/2} \int_0^L Nu dy dz \quad (10)$$

The previously described mathematical model is written by a FORTRAN program. The control volume finite difference method is used to discretize governing equations [2-4, 8], respectively. The central-difference scheme is used for treating convective terms while the fully implicit procedure is used to discretize the temporal derivatives. The grids are considered uniform in all directions with clustering nodes on boundaries. The successive relaxation iteration scheme is used to solve the resulting non-linear algebraic equations.

A computer program written for a regular grid was improved to handle the irregularly shaped computational domain using the blocked-off method as described in [22]. In this technique, the whole region is divided into two active and inactive (blocked-off regions) parts, fig. 2. By this technique, the surface of inclined step in the present analysis is approximated by a series of fine cubic steps. It is obvious that using fine grids in the interface region between active and inactive zones causes to have an approximated boundary which is more similar to the true boundary. According to the blocked-off technique, known values of the dependent variables must be established in all inactive control volumes. If the inactive region

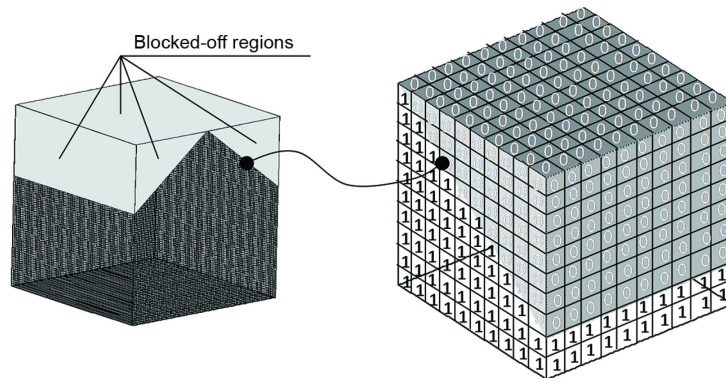


Figure 2. Blocked-off region in a regular grid

represents a stationary solid boundary as in the case, the velocity components in that region must be equal to zero, and a known temperature (isothermal boundaries) must be established in the inactive control volumes. The control volumes, which are inside the active region, are designated as (1) and otherwise they are (0). The time step (10^{-4}) and spatial mesh ($81 \times 81 \times 81$) are utilized to carry out all the numerical tests. The solution is considered acceptable when the following convergence criterion is satisfied for each step of time:

$$\sum_i^{1,2,3} \frac{\max |\psi_i^n - \psi_i^{n-1}|}{\max |\psi_i^n|} + \max |T_i^n - T_i^{n-1}| \leq 10^{-4} \quad (11)$$

Validation

Validation of the code is performed against two published studies. Thus, results are compared with studies of Wakashima and Saitho [23] for differentially heated cubic cavity and $Pr = 0.71$ and listed in tab. 1. As seen from the table that obtained results is acceptable when compared with literature.

Table 1. Comparison of present results with the 3-D results [23] for differentially heated cubic cavity and $Pr = 0.71$

Ra	Authors	ψ_z (center)	ω_z (center)	$V_{x \max}$ (y)	$V_{y \max}$ (x)	Nu_{av}
10^4	Present work	0.05528	1.1063	0.199 (0.826)	0.221 (0.112)	2.062
	Wakashima and Saitho [23]	0.05492	1.1018	0.198 (0.825)	0.222 (0.117)	2.062
10^5	Present work	0.034	0.262	0.143 (0.847)	0.245 (0.064)	4.378
	Wakashima and Saitoh [23]	0.03403	0.2573	0.147 (0.85)	0.246 (0.068)	4.366
10^6	Present work	0.01972	0.1284	0.083 (0.847)	0.254 (0.032)	8.618
	Wakashima and Saitho [23]	0.01976	0.1366	0.0811 (0.86)	0.258 (0.032)	8.6097

Results and discussion

Trajectories of particles for different Rayleigh number values are illustrated in fig. 3. It is noted that Prandtl number is fixed at $Pr = 0.71$ for whole work and Grashof number is changed to obtain different Rayleigh number. In this work, Rayleigh number is the main parameter which is changed from 10^3 to 10^6 . The numerical result shows an incoming air-flow at the lower level opening in the right heated façade while the internal hotter air is pushed

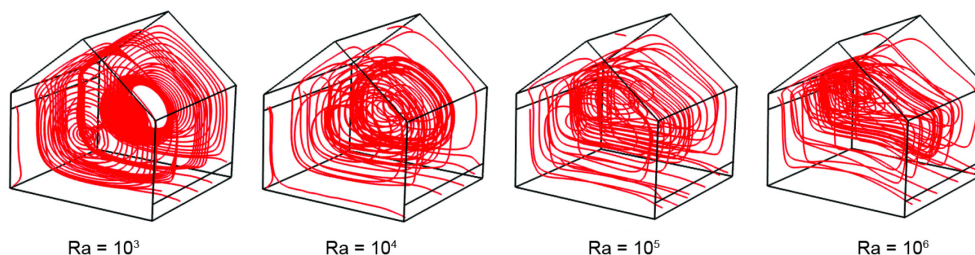


Figure 3. Particles trajectory for different Rayleigh number values

outwards through the upper level opening near the roof top in the opposite cooled façade. Therefore, as seen from the figure, particles circulate in clockwise direction forming one vortex flow structure and a spiraling transversal ordered flow. By increasing Rayleigh number, the transversal flow becomes more and more disordered.

Figure 4, presents the velocity vector projections in the central plan of the cavity ($z = 0.5$) for different Rayleigh number values. For small values of this parameter ($Ra \leq 10^4$), the flow is thermally dominated by conduction mode of heat transfer with only one clockwise rotating thermal vortex whose center is located in the middle of the enclosure and then is pushed to the left side for $Ra = 10^5$. By increasing Rayleigh number ($Ra = 10^6$) and due to domination of natural convection two vortex were formed inside the main vortex and the flow becomes a two-inner vortex structure.

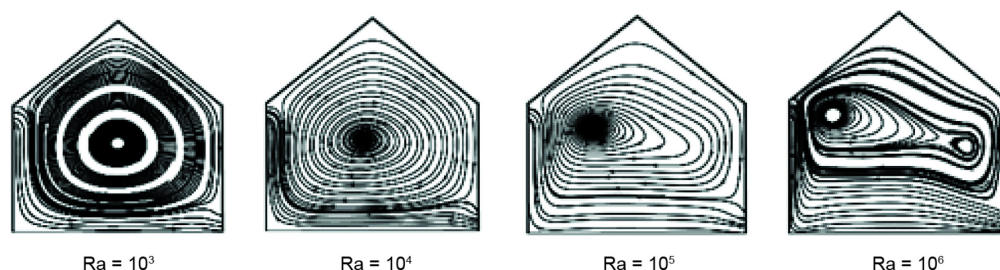


Figure 4. Projection of streamlines in the central plan of the cavity ($z = 0.5$) for different Rayleigh number values

The main vortex is elongated with widening the area occupied by the incoming air-flow due to strong velocity as it can be seen in figs. 5 and 6 and it becomes thinner for $Ra = 10^6$.

Figures 5 and 6 illustrate the 3-D distribution of the outlet velocity modulus and the inlet velocity modulus, respectively, for: (a) $Ra = 10^4$ and (b) $Ra = 10^6$. It is clear that the 3-D character is more pronounced near the corners. In fact we note an almost flattened non-uniform distribution in the middle of the outlet, whereas a peak in the middle of the inlet is found with non-uniform velocity distribution. It can be seen also that increasing Rayleigh number increases considerably the velocity of incoming air-flow due to strong buoyancy force intensity.

Figure 7 presents the iso-surfaces of temperature for different Rayleigh number values. When heat transfer is dominated by conduction mode ($Ra = 10^3$), the isotherms present vertical stratifications in the upper part of the greenhouse and excessive temperature gradient near the lower part of the hot wall and the upper part of the cold wall. By increasing Rayleigh number ($Ra \geq 10^5$) this stratification persists only near active walls whereas isotherms in the central part of the cavity, became horizontally uniform and stably stratified in the vertical direction.

The temperature distribution in the greenhouse is determined by the isotherms structures, fig. 8. Let us note that the isotherms are perpendicular to the adiabatic walls. For low Rayleigh numbers, the isotherms are almost parallel, and become increasingly corrugated as the Rayleigh number increases, which explains that the heat transfer is accentuated. It is also noted that heated air near the hot wall is increasingly driven by the incoming air-flow at the lower part of the greenhouse making horizontal isotherms and results in dead zone near the apex angle on the top. Indeed, the increase of Rayleigh number induces a rise in the buoyancy

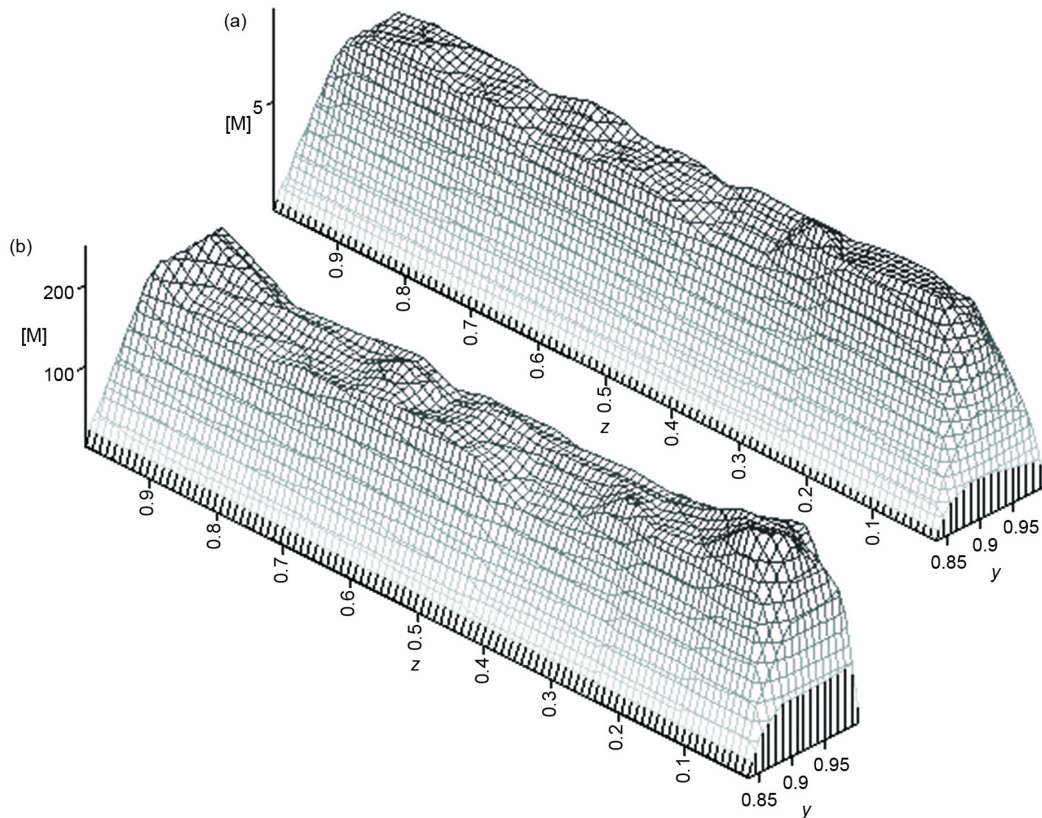


Figure 5. Outlet velocity modulus; (a) $Ra = 10^4$, (b) $Ra = 10^6$

forces which means an increase in the air velocity and consequently, the extraction of a larger heat quantity. As can be seen, the inclination of isotherms near the adiabatic surfaces is more important as Rayleigh number increases and the top of the greenhouse remains cold and less ventilated with this openings configuration.

The isotherms and streamlines structures, figs. 7 and 8, do not give exact information on the effect of Rayleigh number on the total heat transfer inside the greenhouse. For this reason, we present the average Nusselt number which characterizes the heat transfer from the hot wall towards the greenhouse, fig. 9. Note that the average Nusselt number increases with increasing the Rayleigh number. Indeed, by increasing Rayleigh number to 10^5 , the fluid flow intensifies and the thermal energy transport from the hot wall increases due to the enhancement of convection. Consequently, there is an increase in heat transfer rate to the fluid at $Ra \geq 10^4$.

Entropy generation gives an idea on losses due to heat transfer and fluid friction. Entropy generation is calculated from its definition as given in eqs. (7) and (8). In these equations, irreversibility coefficient is taken as $\Phi = 10^{-4}$. Velocities and temperatures are obtained from the solution of governing equations. Figure 10 illustrates the 3-D distribution of the total entropy generation, and it is clear that the 3-D character is more pronounced for $Ra = 10^4$ (on the left column) than the case of $Ra = 10^6$ (on the right column). The 3-D character exists for both S_{th} and S_{fr} . This is also noticed that for low values of Rayleigh number the generated

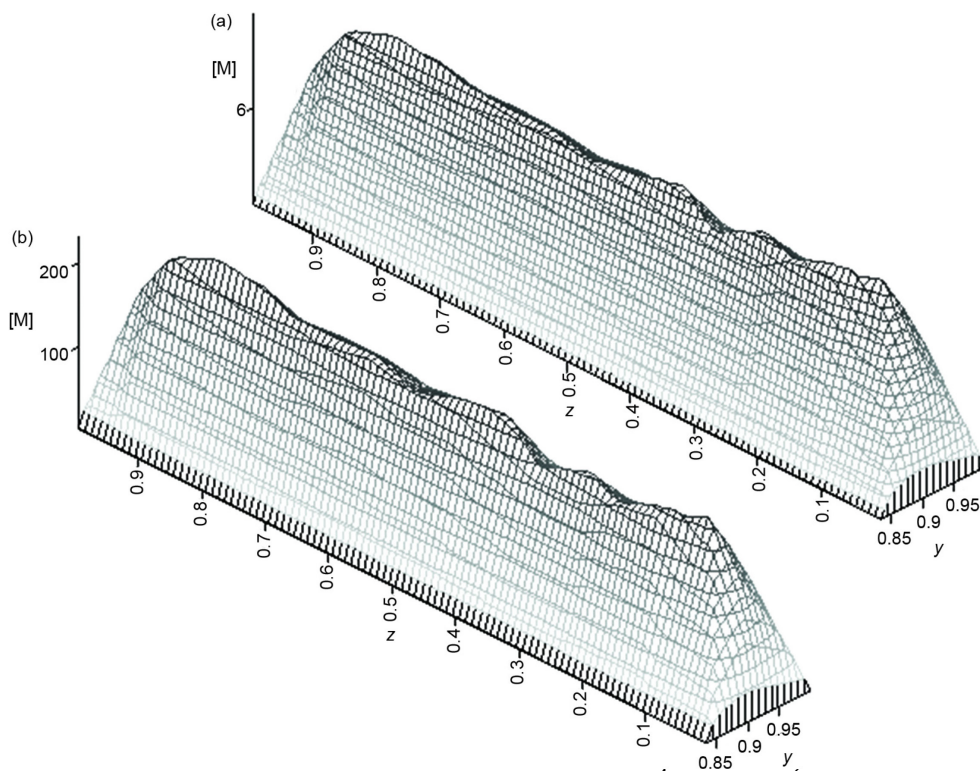


Figure 6. Inlet velocity modulus; (a) $Ra = 10^4$, (b) $Ra = 10^6$

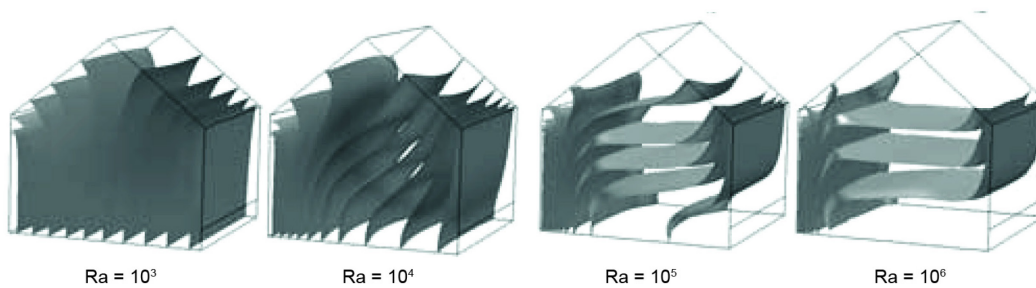


Figure 7. Iso-surfaces of temperature for different Rayleigh number values

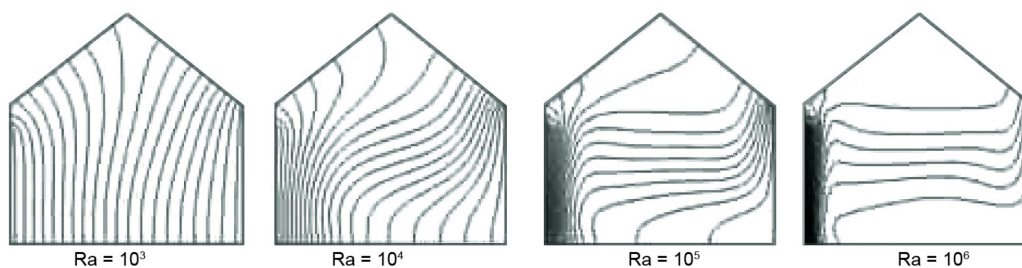


Figure 8. Projection of isotherms in the central plan of the cavity ($z = 0.5$) for different Rayleigh number values

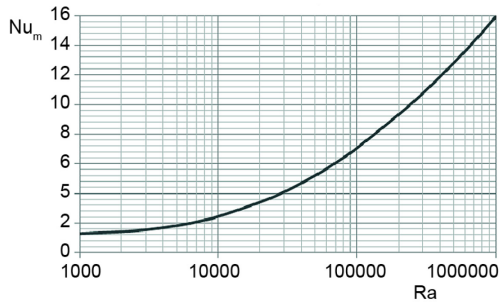


Figure 9. Variation of mean Nusselt number on hot wall with Rayleigh number

entropy covers the entire greenhouse. By increasing Ra , the generated entropy concentrates (locates itself) along active walls. This can explain the boundary-layer phenomenon met for the great Rayleigh numbers. The 3-D behavior of the distribution of the generated entropy is important for only the S_{fr} . The maximum of S_{th} is located in the region near the center of active walls.

Figure 11 shows entropy generation due to heat transfer, entropy generation due to friction and total entropy generation. As seen from this figure, entropy generation remains con-

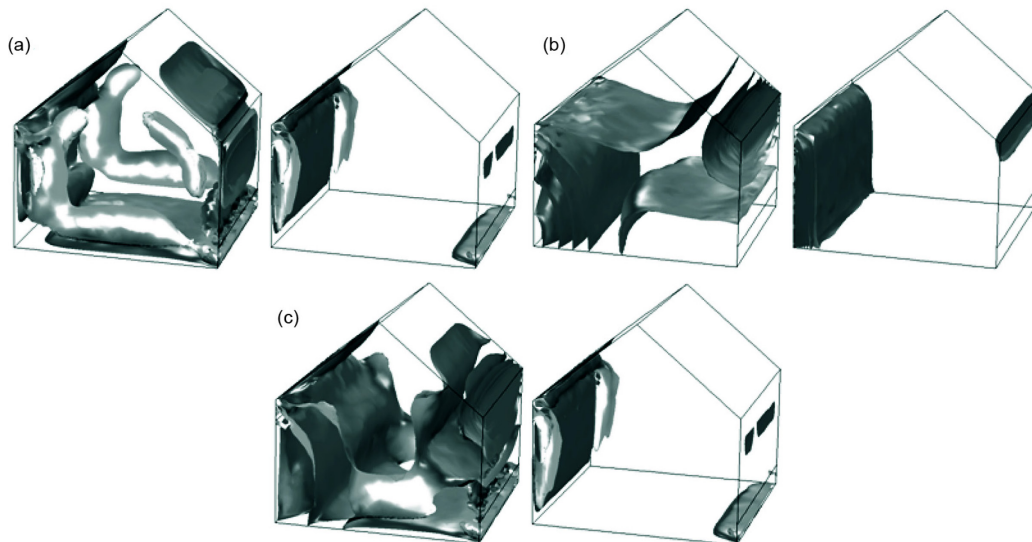


Figure 10. Iso-surfaces of entropy generation for $Ra = 10^4$ (on the left column) and for $Ra = 10^6$ (on the right column); (a) entropy generation due to fluid friction, (b) entropy generation due to heat transfer, (c) total entropy generation for $\Phi = 10^{-4}$

stant for lower values of Rayleigh number and increases gradually for $Ra \geq 10^4$. Entropy generation due to friction and total entropy generation follow same trend for higher values of Rayleigh number where the irreversibility due to fluid friction dominates.

Conclusions

In the present work, we attempt to introduce a numerical approach for investigating the ventilation efficiency of greenhouses under low-wind-speed conditions. For this reason, we

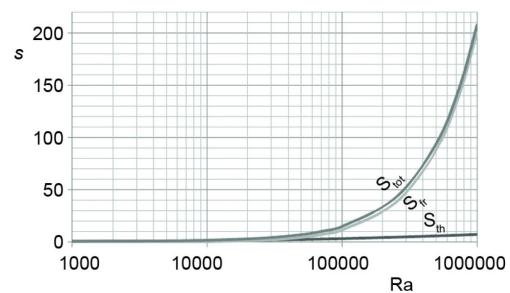


Figure 11. Variation of entropy generation with Rayleigh number

analyzed the ventilation behavior of greenhouse structures when air temperature differences constitute the main driving force of the flow-*buoyancy effect*. Most of the greenhouse designers usually neglect to optimize the greenhouse thermally driven ventilation since low-wind-speed conditions are rare in agricultural areas. Nevertheless, low-wind-speeds frequently coincide with high temperatures, when high ventilation efficiency is mostly required. Numerical CFD simulations offer a detailed picture of the temperature spatial distribution and the air-flow field. Some important findings can be drawn as follows.

- Using asymmetric opening positions improve the natural ventilation and facilitate the occurrence of buoyancy induced upward cross air-flow (low-level supply and upper-level extraction) inside the greenhouse.
- For small values of Rayleigh number ($Ra \leq 10^4$), the flow is thermally dominated by conduction mode of heat transfer with only one clockwise rotating thermal vortex whose center is located in the middle of the enclosure and then is pushed to the left side for $Ra = 10^5$.
- By increasing Ra ($Ra = 10^6$) and due to domination of natural convection two cells were formed inside the main cell and the flow becomes a two-inner vortex structure.
- Heated air near the hot wall is increasingly driven by the incoming air-flow at the lower part of the greenhouse making horizontal isotherms and results in dead zone near the apex angle on the top of the greenhouse which remains cold and less ventilated with this openings configuration.
- By increasing Rayleigh number to 10^5 , the fluid flow intensifies and the thermal energy transport from the hot wall increases due to enhanced convection. Consequently, there is an exponential increase in the average Nusselt number at $Ra \geq 10^4$.
- For $Ra = 10^6$, the generated entropy concentrates along active walls which explains the boundary-layer phenomenon met for the great Rayleigh numbers.
- Entropy generation due to friction and total entropy generation follow same trend for higher values of Rayleigh number where the irreversibility due to fluid friction dominates.

These conclusions can bring useful information to designers of greenhouse frames or greenhouse control systems. However, we have to keep in mind that the CFD results discussed in this paper deal with empty greenhouses. Consequently, they provide only a rough picture of the ventilation flow in actual greenhouses, where the plants and the internal structural elements affect the internal air-flow. Further investigation is required for achieving a simplified and realistic representation of these blocking elements in CFD simulations.

Acknowledgment

The authors would like to thank the Academic Research Dean of University of Hail Saudi Arabia for supporting the research project.

Nomenclature

g	– gravitational acceleration, [ms^{-2}]	S_{gen}'	– generated entropy
k	– thermal conductivity, [$\text{Wm}^{-1}\text{K}^{-1}$]	T^*	– dimensionless temperature, [$= (T' - T'_c)/(T'_h - T'_c)$]
L	– greenhouse width, [m]	T'_c	– cold temperature, [K]
N_s	– local generated entropy	T'_h	– hot temperature, [K]
Nu	– local Nusselt number	ΔT^*	– dimensionless temperature difference
\vec{n}	– unit vector normal to the wall	\bar{t}	– dimensionless time, ($= t'\alpha/L^2$)
Pr	– Prandtl number	\vec{V}	– dimensionless velocity vector, ($= \vec{V}'L/\beta$)
\vec{q}	– heat flux vector, [Wm^{-2}]		
Ra	– Rayleigh number		

x, y, z – dimensionless Cartesian co-ordinates, ($x'/L, y'/L, z'/L$)

Greek symbols

α – thermal diffusivity, [m^2s^{-1}]
 β – thermal expansion coefficient, [K^{-1}]
 μ – dynamic viscosity, [$kgm^{-1}s^{-1}$]
 ν – kinematic viscosity, [m^2s^{-1}]
 ρ – density, [kgm^{-3}]
 ϕ – irreversibility coefficient
 ϕ' – dissipation function

$\bar{\Psi}$ – dimensionless vector potential, ($= \bar{\Psi}/\alpha$)
 ω – dimensionless vorticity, ($= \omega' a/L^2$)

Subscripts

fr – friction
 m – mean
 th – thermal
 tot – total
 x, y, z – Cartesian co-ordinates

Superscript

' – dimensional variable

References

- [1] Okushima, L., et al., A Support System for Natural Ventilation Design of Greenhouse Based on Computational Aerodynamics, *Acta Horticulturae*, 248 (1989), 13, pp. 129-136
- [2] Lamrani, M. A., et al., Airflow and Temperature Patterns Induced in a Confined Greenhouse, *Journal of Agricultural Engineering Research*, 78 (2001), 1, pp. 75-88
- [3] Montero, J. I., et al., Computational Fluid Dynamic Modelling of Night-Time Energy Fluxes in Unheated Greenhouses, *Acta Horticulturae*, 691 (2005), 48, pp. 403-410
- [4] Boulard, T., et al., Characterization and Modelling of the Air Fluxes Induced by Natural Ventilation in a Greenhouse, *Journal of Agricultural Engineering Research*, 74 (1999), 2, pp. 135-144
- [5] Sase, S., et al., Wind Tunnel Testing on Airflow and Temperature Distribution of a Naturally Ventilated Greenhouse, *Acta Horticulturae*, 148 (1984), 42, pp. 329-336
- [6] Mistriotis, A., et al., Computational Analysis of Ventilation in Greenhouses at Zero and Low-Windspeed, *Agricultural and Forest Meteorology*, 88 (1997), 1-4, pp. 121-135
- [7] Montero, J. I., et al., Effect of Ventilator Configuration on Wind Driven Ventilation in a Crop Protection Structure for the Tropics, *Journal of Agricultural Engineering Research*, 80 (2001), 1, pp. 99-107
- [8] Kittas, C., et al., Quantification of the Ventilation of a Greenhouse with a Roof Opening, *Agricultural and Forest Meteorology*, 77 (1995), 2, pp. 95-111
- [9] Ould Khaoua, S. A., et al., Analysis of Greenhouse Ventilation Efficiency with CFD, *Biosystems Engineering*, 95 (2006), 1, pp. 83-98
- [10] Bournet, P. E., et al., Numerical Prediction of the Effect of Vents Arrangements on the Ventilation and Energy Transfers in a Multispan Glasshouse Using a Bi-Band Radiation Model, *Biosystems Engineering*, 98 (2007), 2, pp. 224-234
- [11] Bournet, P. E., et al., Effect of Roof and Side Opening Combinations on the Ventilation of a Glasshouse Using Computer Simulations, *Transactions of the ASABE, American Society of Agricultural and Biological Engineers*, 50 (2007), 1, pp. 201-212
- [12] Lee, I. B., et al., Evaluation of Structural Characteristics of Naturally Ventilated Multi-Span Greenhouse Using Computer Simulation, *Japan Agricultural Research Quarterly*, 34 (2000), 4, pp. 247-256
- [13] Kacira, M., et al., A CFD Evaluation of Naturally Ventilated Multi-Span, Sawtooth Greenhouses, *Transaction of the ASAE*, 41 (1998), 3, pp. 833-836
- [14] Kacira, M., et al., Effect of Vent Configuration and Wind Speed on Three-Dimensional Temperature Distributions in a Naturally Ventilated Multi-Span Greenhouse by Wind Tunnel Experiments, *Acta Horticulturae*, 801 (2008), 41, pp. 393-400
- [15] Lo, L. J., Novoselac, A., Cross Ventilation with Small Openings: Measurements in a Multi-Zone Test Building, *Build environ*, 57 (2012), Nov., pp. 377-386
- [16] Aich, W., et al., Numerical Analysis of Natural Convection in a Prismatic Cavity, *Thermal Science*, 15 (2011), 2, pp. 437-446
- [17] Oztop, H. F., et al., Numerical Study of Three-Dimensional Combined Buoyancy and Thermocapillary Convection and Evaluation of Entropy Generation, *International Journal of Numerical Methods for Heat & Fluid Flow*, 24 (2014), 1, pp. 148-168
- [18] Kolsi, L., et al., Second Law Analysis in a Three Dimensional Lid-Driven Cavity, *International Communications in Heat and Mass Transfer*, 38 (2011), 10, pp. 1376-1383
- [19] Blocken, B., 50 years of Computational Wind Engineering: Past, Present And Future, *J Wind Eng Ind Aerodyn*, 129 (2014), June, pp. 69-102

- [20] Blocken, B., et al., Application of Computational Fluid Dynamics in Building Performance Simulation for the Outdoor Environment: An Overview, *J Build Perform Simul*, 4 (2011), 2, pp. 157-184
- [21] Kolsi, L., et al., Effect of an External Magnetic Field on the 3-D Un Steady Natural Convection in a Cubical Enclosure, *Numerical Heat Transfer Part A*, 51 (2007), 10, pp. 1003-1021
- [22] Patankar, S. V., *Numerical Heat Transfer and Fluid Flow*, Taylor & Francis, Philadelphia, Penn., USA, 1981
- [23] Wakashima, S., Saitoh, T. S., Benchmark Solutions for Natural Convection in a Cubic Cavity Using the High-order Time-Space Method, *Int. J. Heat Mass Transfer*, 47 (2004), 4, pp. 853-864

